



Universiteit  
Leiden  
The Netherlands

## Surface temperature and the dynamics of H<sub>2</sub> on Cu(111)

Smits, B.

### Citation

Smits, B. (2023, July 4). *Surface temperature and the dynamics of H<sub>2</sub> on Cu(111)*. Retrieved from <https://hdl.handle.net/1887/3628423>

Version: Publisher's Version

License: [Licence agreement concerning inclusion of doctoral thesis in the Institutional Repository of the University of Leiden](#)

Downloaded from: <https://hdl.handle.net/1887/3628423>

**Note:** To cite this publication please use the final published version (if applicable).

# Beyond the static corrugation model

This chapter is based on Smits, B.; Somers, M. F. Beyond the static corrugation model: Dynamic surfaces with the embedded atom method. *The Journal of Chemical Physics* **2021**, *154*, 074710, DOI: [10.1063/5.0036611](https://doi.org/10.1063/5.0036611)

## Abstract

The D<sub>2</sub> on Cu(111) system has for many years been one of the major benchmark systems for surface scientists. Generating surface configurations using the embedded atom method (EAM), we investigate the quality of the chemically accurate static corrugation model (SCM) for including surface temperature effects, with a focus on the random displacement approach to its distorted surface generation. With this EAM potential, we also treat the Cu(111) surface of our system fully dynamically and shed a further light on not only the quality of the SCM sudden approach, but also the limited effect of energy exchange with the surface. Reaction and (in)elastic scattering probability curves, as well as simulated time-of-flight spectra, show good agreement with both earlier works and experimental results, with surface reactions showing a preference for surface atoms displaced away from the incoming molecule. The good agreement with the non-static surface model also further establishes the limited effect of energy exchange on not only the reaction, but also on the elastic and inelastic scattering probabilities, even though some molecular translational energy is deposited into the surface.

### 3.1 Introduction

For many years, theoreticians and experimentalists have been working on describing gas-solid surface reactions[1–3]. These are especially of interest due to their importance in many (industrial) processes, such as the Haber-Bosch process[4] or H<sub>2</sub> dissociation for hydrogen engines[5]. To best describe these processes the reaction mechanisms are broken up into simple elementary reaction steps. Studying of individual steps would then allow for a very accurate description of the full catalytic process.

Our system of choice for this chapter is the D<sub>2</sub> dissociation on a Cu(111) surface. This system is one of the model systems for surface scientists, with a lot of available experimental[6–13] and theoretical[2, 14–19] data. In the past, theoretical work was often performed using the Born-Oppenheimer and the static surface (BOSS) approach, where surface atoms are assumed to be fully static, and the electron and nucleus dynamics are assumed to be separated. Here the *ab initio* density functional theory (DFT) results are often fit to a 6D potential energy surface (PES), using an approach such as the corrugation reducing procedure (CRP)[20].

Making use of this method, Díaz *et al.*[14] developed the specific reaction parameter (SRP) approach. By linearly combining two different DFT functionals, one overestimating and one underestimating the dissociation barrier, this work was able to reproduce experimental molecular beam experiments of H<sub>2</sub> of Cu(111) with an error of less than 1.0 kcal/mol[21].

Although good results were obtained using these methods, the surface slab was kept at its ideal, “0 K” configuration, whereas experiments are often performed at higher temperatures[22]. To allow for the PES to take into account surface temperature effects, Wijzenbroek and Somers coined the static corrugation model (SCM)[23]. In this model, surface slab atoms are displaced from the ideal lattice, but kept static. It was theorised such an approach would work well for a H<sub>2</sub> or D<sub>2</sub> on copper system, which is expected to have only limited energy transfer, both due to the mass mismatch between hydrogen and copper atoms as well as the relatively slow speed of the thermally equilibrated copper surface atoms. A two body (H-Cu) coupling potential ( $V_{coup}$ ) was introduced to describe the changes in the PES due to these displacements. This coupling potential was fitted to a data set of surface configurations obtained using DFT calculations with the SRP48 exchange-corellation functional[17]. This initial approach to the SCM showed great agreement with *ab initio* molecular dynamics (AIMD) calculations using the same DFT functional[17]. Furthermore, it resulted in better agreement with experiment than originally achieved with the SRP-BOSS approach, although the limited size of the data

set also showed a sizeable error in the H-Cu coupling potential. To improve upon the SCM, Spiering *et al.*[24] expanded the SCM to an effective three-body potential, by including the H-H distance into the coupling potential. Furthermore, the data set for fitting was greatly expanded, which reduced the RMSE of the fitted three-body coupling potential to 29.4 meV, compared to 66.6 meV for the two-body potential of the initial study. To generate these statically distorted surface slabs for the SCM, each surface atom is displaced using a normal distribution based on experimentally determined Debye-Waller factor for a specific modelled temperature. The interlayer distances are instead taken directly from experiment.

It is, however, still unclear if such a random displacement generates physically relevant surface slabs. Therefore, we elected to expand upon the SCM approach by generating surface slabs using a highly accurate embedded atom method (EAM) potential as described by Sheng *et al.*[25]. This potential has been shown to accurately describe not only lattice constants and phonon dispersion curves but also thermal expansion of the bulk metal and the FCC copper surface slabs[25]. These surface slabs can then be used in combination with the SCM coupling potential to generate dissociation curves and simulated time-of-flight spectra. A comparison of these curves between these randomly displaced surfaces and EAM generated surfaces should allow us to validate the quality of this earlier work.

To further expand our model, we can even use the EAM potential to dynamically describe our copper surface during dissociation simulations. Here, the SCM coupling potential does not only describe the effect of the surface on the  $D_2$ , but also describes the effect of the  $D_2$  on the surface, effectively allowing for energy exchange to be introduced in our system. Energy exchange has long been theorised to not be very relevant for dissociation probabilities in the  $H_2$  on Cu(111) system, due to the large mass mismatch. In this work, however, we will be able to investigate its effect directly, by comparing results from both a static and dynamic surface using exactly the same potentials.

With the SCM approach, switching to another surface facet of the  $D_2$ /Cu system would only require a new CRP BOSS PES. This contrasts other approaches, like high dimensional neural network potentials (HD-NNPs), which would need a new extended training set to be fit to. The SCM coupling potential is also generic in that respect, as it has been shown that the underlying DFT functional of  $V_{coup}$  is transferable between the  $H_2$  on Cu(111) and  $H_2$  Cu(100) systems[26]. Moreover, recently a  $H_2$  on Cu(211) stepped CRP BOSS PES has been constructed also with the SRP48 DFT functional[27, 28].

The transferability of the SCM approach to surface slabs of a different transition metal, such as Pt or Ag, will still require additional work. Although

3

this can be greatly reduced by using one of the many (CRP) PESs[3] and EAM potentials[25] available in literature, reducing it to merely fitting a new SCM coupling potential. Of special interest would be those systems with an early barrier, as they exhibit a relatively small amount of corrugation, and a large mass mismatch between the  $D_2$  and the metal. For those systems where no well performing GGA-level DFT functionals are available, like Pd[29], another first principles approach would be required to obtain a data set to fit the SCM coupling potential. Similarly, a new data set would be required to fit an HD-NNP for such a new system, which can generally also require extensive DFT data sets[30].

In this chapter, however, we aim to investigate two assumptions made in previous studies. Primarily, we will validate the physical relevance of the SCM random displacement approach to surface slab generation, by comparing the results of  $D_2$  dissociation on such a surface slab to a physically accurate surface slab generated with an EAM potential. Furthermore, we also go beyond the SCM by dynamically treating the metal atoms of the surface slab with this EAM potential. This will allow us to both further investigate the quality of the sudden approximation that lies at the base of the SCM, as well as investigate the importance of energy exchange with the Cu surface for chemisorption and rovibrationally (in)elastic scattering probabilities.

## 3.2 Method

All calculations for this chapter are performed using the quasi-classical dynamics (QCD) approach as described in section 2.2.1, for a variety of initial rovibrational states. The final states of the scattered trajectories are binned using the standard binning method. The time-of-flight spectra presented in 3.3.3 were simulated using fits to the obtained dissociation curves using the LGS functional form, with the required experimental parameters and angular averaging as published in [16].

Results of both the random displacement (RD-SCM) and the MD based EAM-SCM results are included, as well as the moving surface EAM-DCM results. For the EAM-SCM and EAM-DCM results, a database of thermally distorted surface slabs was created using molecular dynamics, and the highly accurate EAM potential for copper as described by Sheng *et al.*[25]. This same database of surface slabs is also used in Chapters 4, 5, and 6 of this thesis.

To be able to perform molecular dynamics, the EAM potential is described using 1001 equidistant data points for the pair, density and embedding functions, which are fitted using cubic splines. A cutoff is used at 0 Å and 6.5 Å for the pair and density functions, and at 0.0 and 1.0 density for the embedding

function. Outside these final spline knots, both the value of the function and its derivative yield 0.

NVT dynamics were run using a Velocity-Verlet algorithm[31] and the Berendsen thermostat[32], while NVE propagation was performed using the Bulirsch-Stoer predictor-corrector algorithm[33].

Step-wise volume scaling was performed to equilibrate the pressure and Cu lattice constant, by running 1 ps of NVT dynamics and storing the virial pressure each step, calculated using[34]

$$P_{vir} = Nk_bT + \frac{1}{2} \cdot \frac{1}{3} \sum_{i \neq j} r_{ij} \cdot F_{ij} \quad (3.1)$$

Here  $N$  is the number of (mobile) surface atoms,  $k_b$  is the Boltzmann constant,  $T$  is the instantaneous surface temperature, and  $r_{ij}$  and  $F_{ij}$  are, respectively, the distance and force between surface atom  $i$  and  $j$ . Due to double counting this dot product is halved. The total average pressure is then divided by a scaling factor of 2500 GPa and used to scale the simulation box volume. This scaling factor was chosen arbitrarily, to ensure the surface is not scaled too fast or too slow.

To ensure this yields satisfactory results, we also determine the pressure from the diagonal components of the virial stress tensor. Both these methods are grounded in theory and should yield in the same values under equilibrated conditions[34].

### 3.2.1 Bulk lattice constant determination

To determine the relaxed bulk lattice constant, a cell of  $7 \times 7 \times 7$  Cu atoms was placed in the optimal FCC lattice structure. Some initial momentum was also included, using a normal distribution based on the modelled surface temperature, to avoid any rapid changes during the initial surface relaxation steps. The minimum image convention is applied in the x, y and z Cartesian directions, Next this slab was propagated in the canonical ensemble (NVT) for 40000 steps with a step size of .005 ps, for a total propagation of 200 ps. Volume rescaling was performed between 40 and 160 ps of this run, scaling every ps to ensure the thermodynamically favoured box volume is attained. To evaluate the quality of this run, the average atom-atom distance, temperature, and the kinetic and potential energy of the bulk copper are calculated each step and stored for evaluation. Next this NVT relaxed bulk is propagated for 250 steps ( $\sim 6$  ps) in the micro-canonical ensemble (NVE), where total propagation time varies due to the use of the Bulirsch-Stoer predictor-corrector

algorithm. Here we again evaluate the stability of our copper based on the temperature, average atom-atom distance, kinetic and potential energies, and the virial pressure and diagonal components of the virial stress tensor. The relaxed bulk lattice constant is finally obtained from the final volume of our box. This is repeated 200 times, each with a unique seed used to generate the initial conditions, to obtain the average bulk lattice constant of this potential for our chosen temperature.

## 3

### 3.2.2 Surface slab generation

To generate surface slabs, we take the calculated bulk lattice constant to generate the initial  $7 \times 7 \times 7$  FCC copper lattice, and again apply some initial momentum from a normal distribution based on the modelled surface temperature. We further repeat all steps for our bulk lattice, as described above, but without applying any volume rescaling.

Then three consecutive layers of our surface slab with the lowest value of  $z$ , for a total of 147 atoms, are set locked to their current positions. The minimum image convention is only applied in the  $x$ - and  $y$ -directions, parallel to the static layers. This new surface slab is then propagated in the canonical ensemble for a total of 250 ps and a step size of 0.0005 ps (50000 steps). It is important to note we do not apply any volume rescaling during these steps, to ensure our static layers properly model the bulk. This does also mean our top layers will exhibit some stress, due to the change in pressure when moving from the bulk to a surface configuration. A short NVE run of 1000 steps ( $\sim 40$  ps) is again used to determine stability of our surface slab.

To ensure the surface slab atoms are always located approximately at the same position, we next attempt to re-center our slab. We perform an NVE dynamics run of 25000 steps ( $\sim 1100$  ps), logging the average position of each atom in the top layer of our surface slab. After this run, we shift our entire slab, including the static bulk-like layers, so that the average position of the entire top layer is found at  $(x, y, z) = (0, 0, 0)$ . With this process completed, we start our final dynamics run to obtain traces of our surface slab positions and momenta. During an NVE dynamics run of 1250 steps, we take a snapshot every 50 steps ( $\sim 2$  ps) of both the surface slab positions and momenta for a total of 25 snapshots each. To obtain a suitable and diverse amount of traces, we repeat this entire surface slab generation scheme 1000 times, for a total of 25000 surface slab positions with matching momenta. These can then be loaded into our SCM dynamics as an alternative to the random displacement approach of the earlier works.

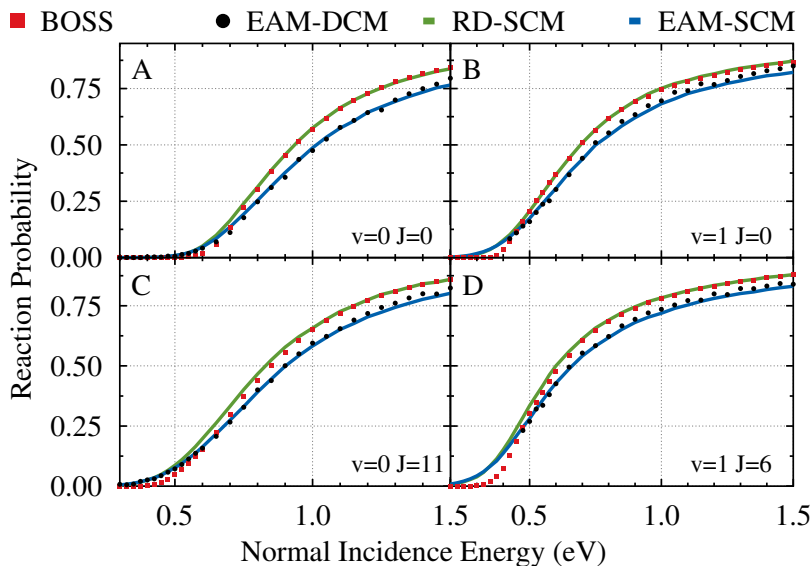


FIGURE 3.1: State-specific reaction probabilities for the  $D_2$  on Cu(111) system and for four different approaches: BOSS (red squares), RD-SCM (green curve), EAM-SCM (blue curve) and EAM-DCM (black circles). For the CM approaches, a modelled surface temperature of 925K was used. Shown are the initial rovibrational states (a)  $v = 0, J = 0$ ; (b)  $v = 1, J = 0$ ; (c)  $v = 0, J = 11$ ; (d)  $v = 1, J = 6$ .

### 3.3 Results and discussion

#### 3.3.1 Reaction probability curves

To validate the quality and physical relevance of the random displacement approach to generating SCM surface slabs (RD-SCM), we will compare the dissociative chemisorption reaction probabilities obtained with this approach to those obtained using surface slabs generated with an EAM potential (EAM-SCM). Also included are dissociation curves for the same dynamics on a moving surface, using the EAM potential to also describe the interactions between the copper atoms. This method we will refer to as the dynamic corrugation model (DCM), using an EAM potential (EAM-DCM). Comparisons between these different methods will give us insight not only in the quality of the RD-SCM generated surface slabs, but also on the effect of energy exchange with our moving surface and the validity of the sudden approach as we use it in the SCM. Finally, we include results of an ideal, “0 K” static surface, which we obtain using the often used BOSS approach. This allows us to investigate the general effect the different models for including surface temperature effects have on the

dissociation curves.

In Figure 3.1, we show the reaction probability curves for several different rovibrational states. As expected, the general trend for all the different approaches are relatively similar. At low incidence energy, the  $D_2$  molecule does not have enough energy to pass over the minimum energy barrier for dissociation, and reaction probability will be minimal. As the normal incidence energy increases so does dissociation probability, until it reaches a maximum, or saturation, value.

The first point of note in this figure is the difference in saturation values between the different approaches. Both the RD-SCM and BOSS methods show a similar saturation at around 0.9, while the EAM-SCM and EAM-DCM approaches both have a lower value at around 0.85, with the EAM-DCM approach always being slightly higher. This could indicate the surface slabs generated with the EAM potential contain somewhat higher maximum barriers compared to those generated through the RD-SCM. These values are, however, very difficult to obtain experimentally and thus is of much less importance for the quality of our model when comparing to experiment[16].

All three CM approaches (RD-SCM, EAM-SCM and EAM-DCM) predict a higher reaction probability than that shown by the BOSS model, yet their curves do not increase as steeply. This broadening of the dissociation curve is generally attributed to surface temperature effects, and has been extensively discussed in earlier work[23, 24, 35]. Both the EAM-SCM and EAM-DCM show a bit more broadening than the RD-SCM approach, although it is harder to quantize due to the lower saturation value. This is especially of note as previous work has shown some indication the width and the saturation value of the dissociation curves are not completely independent[23].

The availability of energy exchange appears to only very limitedly affect our system, as we find great agreement between the static surface approach of the EAM-SCM and the dynamic surface approach of the EAM-DCM. Although earlier studies have shown similar results for  $H_2$ [17, 36–38], this is one of the first examples of a direct and extensive comparison between almost identical methods, one with a dynamic surface and one without.

### 3.3.2 (In-)elastic scattering probabilities

To further analyse our dissociation simulations, we can also look at the rovibrational elastic and inelastic scattering probabilities. In Figure 3.2, we again compare the BOSS (red squares), RD-SCM (green curves), EAM-SCM (blue curves) and EAM-DCM (black circles) methods, now for the elastic [(b), (d), (f),

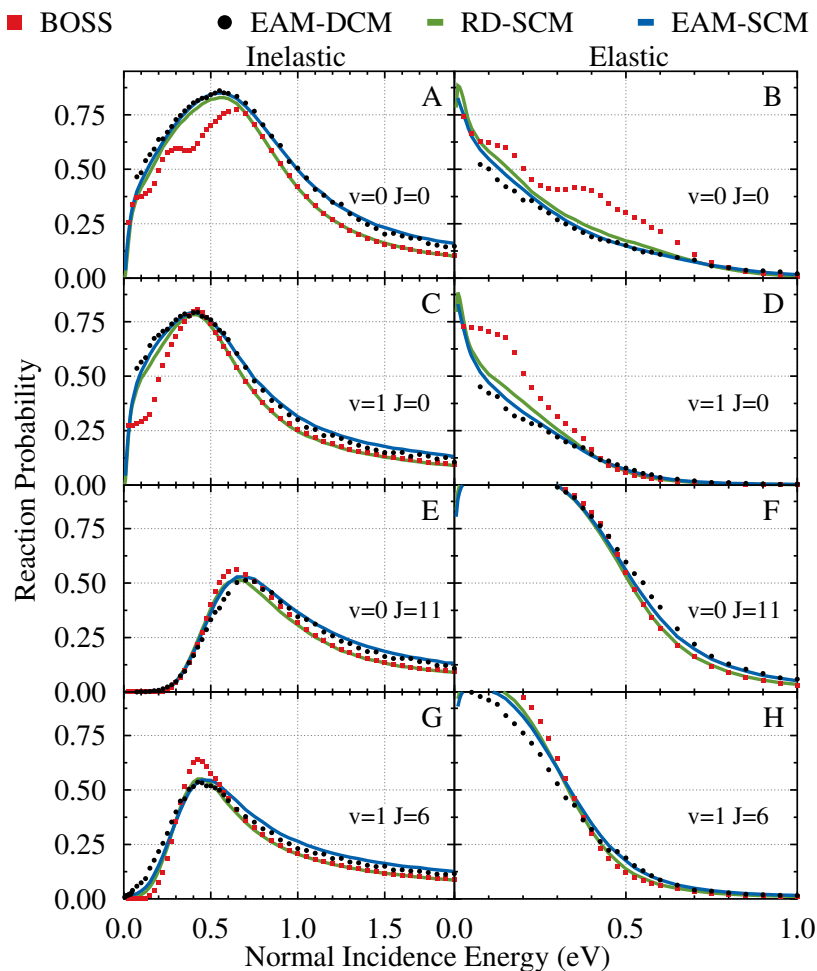


FIGURE 3.2: State-specific, elastic [(b), (d), (f), and (h)] and inelastic [(a), (c), (e), and (g)] scattering probabilities for the  $D_2$  on Cu(111) system and for four different approaches: BOSS (red squares), RD-SCM (green curves), EAM-SCM (blue curves) and EAM-DCM (black circles). For the CM approaches, a modelled surface temperature of 925K was used. Shown are the initial rovibrational states: (a) and (b)  $v = 0, J = 0$ ; (c) and (d)  $v = 1, J = 0$ ; (e) and (f)  $v = 0, J = 11$ ; (g) and (h)  $v = 1, J = 6$ .

and (h)] and in-elastic [(a), (c), (e), and (f)] rovibrational scattering probabilities for the same four initial rovibrational states as discussed before.

In general, we find a preference for elastic scattering at lower incidence energies, where there is not enough energy available within the molecule to reach other rovibrational states. As the kinetic energy of the molecule increases, more and more rovibrational states become available and we find higher and higher probability for inelastic scattering. At very high incidence energies, chemisorption dominates and only limited scattering is observed.

For the rovibrational ground state [(a) and (b)], as well as the vibrationally excited states [(c), (d), (g), and (h)], the BOSS model predicts much higher elastic scattering for the lower incidence energies. Moving to higher energies, we again see almost perfect agreement with the RD-SCM curves and qualitative agreement with the EAM-SCM and EAM-DCM approaches. Surprisingly, this effect is absent for the  $v = 0, J = 11$  state, where the BOSS model shows good agreement with all CM results for all incidence energies.

Agreement between the EAM-SCM and EAM-DCM approaches is again very good, with only minor differences we can partially attribute to the relatively low amount of trajectories ran for the EAM-DCM approach. This further validates the quality of the SCM sudden approach. As the main difference between these two approaches is the possibility of energy exchange between the copper surface and the  $D_2$  molecule, this agreement further enforces our observation of the limited effect of energy exchange on not only the final dissociation results, but also on these rovibrational (in)elastic scattering results. The latter are expected to be more sensitive to details of the PES and to the exchange of energy between  $D_2$  and the surface.

Interestingly, an analysis of the energy exchange in our DCM trajectories does show a small transfer of energy between the copper surface and  $D_2$  molecule. At very low incidence energies ( $< 150$  meV), we find a flow of energy into the  $D_2$  ( $< 10\%$ ), while at higher incidence energies we primarily find a drain of energy into the surface ( $\sim 15\%$ ). This drain of energy was found to be predominantly flowing from the translational energy of the  $D_2$  molecule. Consequently, little difference was found in the rovibrational energy of scattered molecules when comparing the EAM-DCM and EAM-SCM approaches. Furthermore, the average turning point of the scattered molecules was found to be similar between these two methods. This, combined with the minimal differences in (in)elastic rovibrational scattering probabilities, leads us to believe this energy exchange as a result of a mostly mechanical coupling primarily occurs after the scattering event as the  $D_2$  moves away from the surface. We are not aware of any previous works discussing this phenomenon without there being additional particles already on the surface[39], and as such would consider it of great

interest for future work.

The energy exchange at very low incidence energies does appear to affect the final rovibrational state of the scattered molecules. Primarily, it appears to be directly related to the  $z$ -coordinate, as molecules that get closer to the surface obtain a larger amount of energy. It remains, however, a question on how accurate the QCT method is for these very low incidence energies and to what extent quantum dynamical effects like zero point energy conservation, of the molecule and of the surface atoms, play a role[2].

### 3.3.3 Simulated time-of-flight spectra

To better compare our theoretical results to experiment, our reaction probability curves were used to simulate time-of-flight (ToF) spectra. We followed the procedure as outlined in 2.4.2, but also in more detail by Nattino *et al.*[16]. The cut-off function was of the tanh form, with  $t_c$  and  $t_w$  equal to 19.5  $\mu s$  and 6.6  $\mu s$ , respectively. As experimental results are often obtained in the form ToF spectra, and are generally most sensitive for the curve onset of the initial state specific reaction probability curve, we believe ToF spectra are one of the better ways of comparing theoretical results to experimental data, especially when correct and accurate experimental ToF parameters are known and have been published. Thus this work is of great interest, as it both simulated ToF spectra, and fit experimental results using the same expression.

Simulated spectra of a selection of four different rovibrational states for the four theoretical approaches discussed in this work are shown in Figure 3.3. The rovibrational states shown were chosen such that they cover a variety of different excited states, as well as the rovibrational ground state. Furthermore, we also included experimental results from Auerbach *et al.*[8] refit in earlier work, as well as AIMD results, both obtained from the work by Nattino *et al.*[16]. These experimental results were obtained from recombinative desorption experiments of  $D_2$  permeating through the bulk metal to a Cu(111) surface, at a surface temperature of 925 K. As such rely on the applicability of detailed balance[8]. Surface motion effects, for a modelled surface temperature of 925 K, were also included in these AIMD results.

Figures 3.3(a), 3.3(e), and 3.3(i) show our simulated results for the rovibrational ground state. Good agreement is found between the different CM approaches, as was the case for the chemical desorption curves. A slight difference between peak width is observable, with the EAM-SCM approach showing the highest width. The peak location, however, appears to be the same for all three methods. The BOSS model, on the other hand, shows a much more narrow peak with a peak location at a shorter time of flight. The AIMD peak

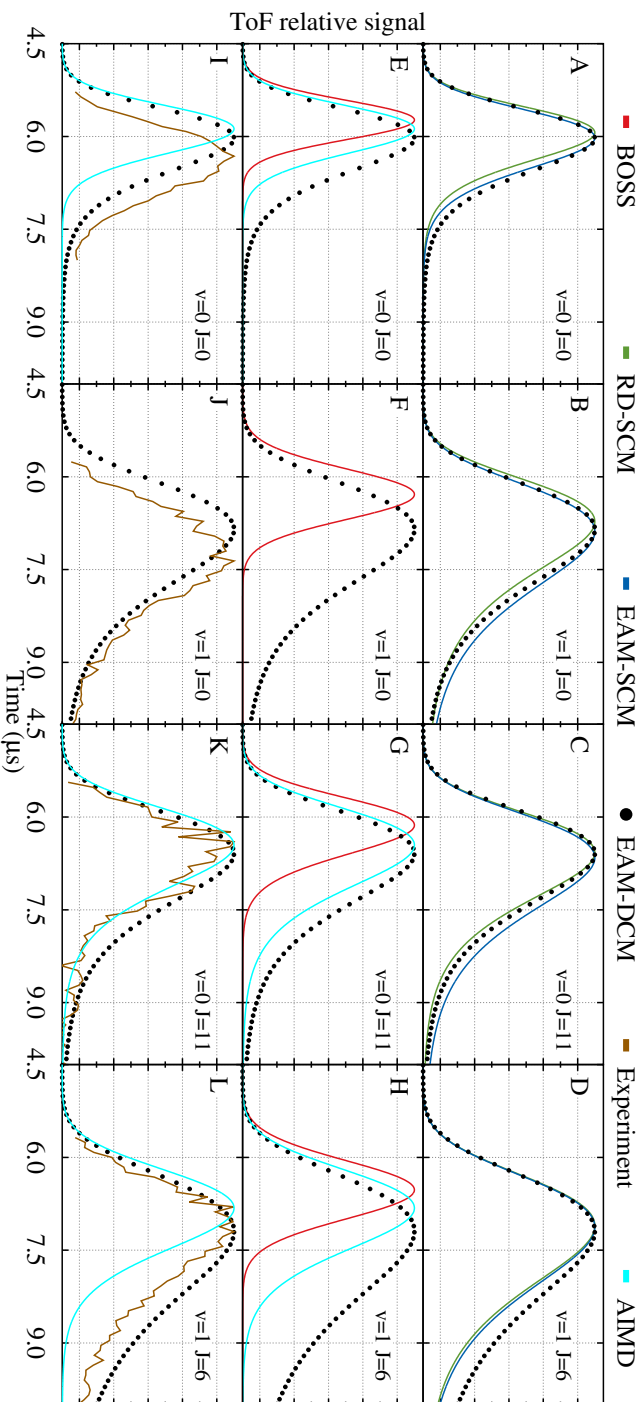


FIGURE 3.3: Simulated time-of-flight spectra for the  $D_2$  on  $Cu(111)$  system. For four different rovibrational states, RD-SCM (green curves), EAM-SCM (blue curves) and EAM-DCM (black circles) are compared to each other [(a)-(d)], as well as to the BOSS approach (red curves) [(e)-(h)], and refitted experimental results (orange curves) [(i)-(l)] and AIMD results (cyan curves) [(e)-(l)] from Nattno *et al.*[16]. For the CM approaches and the AIMD results, a modelled surface temperature of 925K was used, which matches the conditions of the experiment. Shown are the initial rovibrational states: (a), (e), and (i)  $v = 0$ ,  $J = 0$ ; (b), (f), and (h)  $v = 1$ ,  $J = 0$ ; [(e), (g)], and (k)]:  $v = 0$   $J = 11$ ; [(d), (h), and (l)]:  $v = 1$ ,  $J = 6$ .

can be found at approximately the same value as the CM peaks, yet its width is significantly lower. In contrast, looking at the experimental curve, we observe a width similar to that of the CM approaches. The curve is, however, shifted compared to the CM curves, showing a peak location at a higher time of flight.

A similar thing can be observed in Figs. 3.3(b), 3.3(f), and 3.3(j) for the vibrationally excited  $v = 1$ ,  $J = 0$  state. Unfortunately, however, no AIMD data was available for this state. The width for the three CM approaches is once again similar and close to that of the experimental results. Peak location also shows similar results, with the CM approaches underestimating that of the experiment. The BOSS model shows the worst agreement, with a much narrower peak and a peak height about twice as far from experiment.

Moving to the rotationally excited states in Figure 3.3(e)-(h), we again see that the BOSS model yields both the narrowest peak, as well as the lower time-of-flight for the peak. The different CM approaches show peaks at the highest time of flight, each with approximately the same value. The experimental results are found somewhere between these peaks, with a width closer to that of the CM results. AIMD results for these curves are a bit mixed, as the agreement for the  $v = 0$ ,  $J = 11$  state appears to be almost perfect, while agreement with the  $v = 1$ ,  $J = 6$  experimental data is much worse.

Overall, we see improved agreement with experiment when including the SCM and DCM approaches, regardless of which variation. RD-SCM, EAM-SCM, EAM-DCM all show very similar results, with RD-SCM always showing the narrowest peak of the three. Due to the nature of simulating the time-of-flight spectra, however, small variations are expected. The results when using the BOSS model showed the narrowest peaks as well as the shortest time-of-flight for each rovibrational state we investigated, often well below the value found in experiment. This matches findings from earlier work[16].

### 3.3.4 Effect of RD-SCM on atom displacement

In an attempt to directly compare the randomly generated and EAM generated surface slabs, we investigated the displacements of each individual surface slab atom for every Cartesian coordinate. Only those atoms within the SCM cutoff distance of 16 bohrs ( $\sim 8.47$  Å) were included in these results. As discussed in section 2.3.1 of Chapter 2, the RD-SCM approach makes use of the Debye-Waller factor to calculate the standard deviation for the Gaussian displacement of each surface atom. The EAM-SCM approach instead uses surface slabs simulated through another potential, in our case the EAM. Assuming the simulation attains a proper thermodynamic equilibrium, this approach should also result in a Gaussian distribution for our displacements.

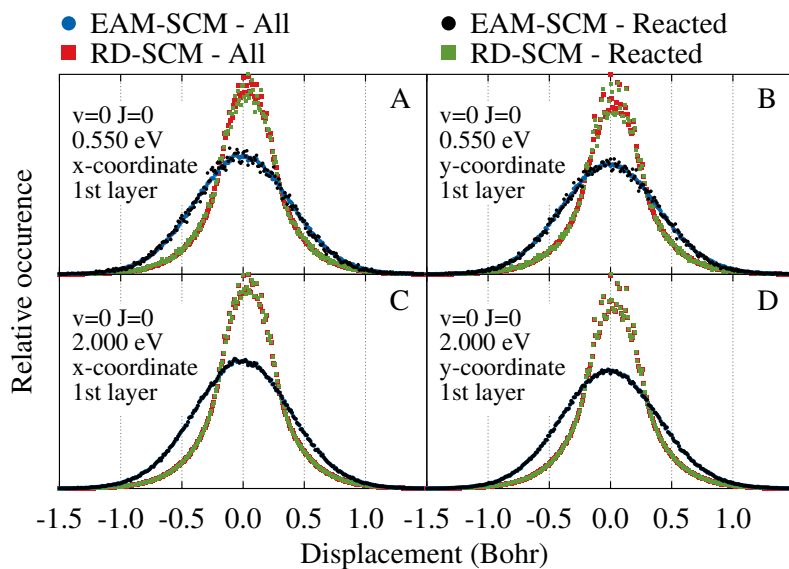


FIGURE 3.4: Surface slab atom displacement at a modelled surface temperature of 925 K relative to the ideal, 0 K lattice. Only those atoms in the first surface layer are included for those trajectories ran on the rovibrational ground state. Included are the displacements both for those trajectories that reacted, and for all trajectories ran for RD-SCM, green and red squares respectively, and EAM-SCM, black and blue circles respectively. Displacements are shown for  $D_2$  normal incidence energies of 0.550 eV [(a) and (b)] or 2.000 eV [(c) and (d)], separating the x-coordinate [(a) and (c)] and y-coordinate [(b) and (d)].

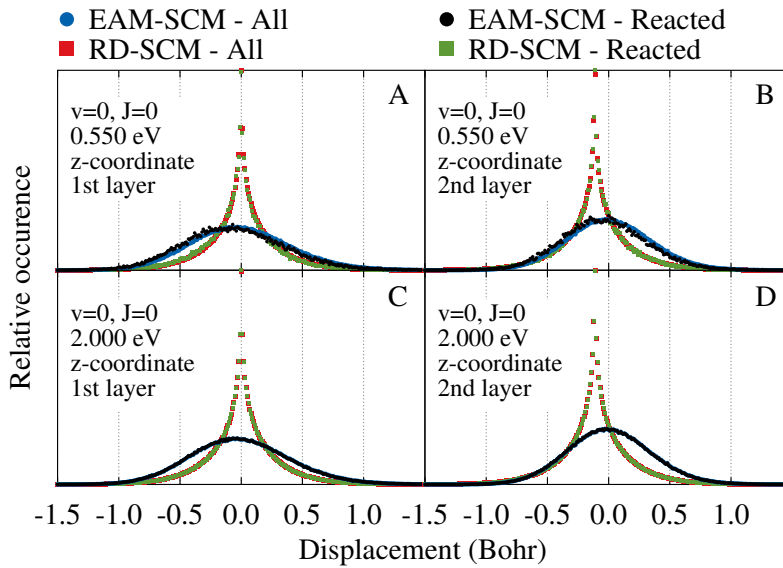


FIGURE 3.5: Surface slab atom displacement at a modelled surface temperature of 925 K relative to the ideal, 0 K lattice. Only those trajectories ran on the rovibrational ground state are shown. Included are the displacements both for those trajectories that reacted, and for all trajectories ran for RD-SCM, green and red squares respectively, and EAM-SCM, black and blue circles respectively. Displacements are shown for  $D_2$  normal incidence energies of 0.550 eV [(a) and (b)] or 2.000 eV [(c) and (d)], separating the x-coordinate [(a) and (c)] and y-coordinate [(b) and (d)].

In Figure 3.4, we outlined the displacements in the x- [(a) and (c)] and y-direction [(b) and (d)] both at the onset of the reaction probability curve [(a) and (b)] as well as at the saturation value [(c) and (d)]. Only those surface slab atoms at the top layer were included in these results. Separate curves were also included for only those trajectories where the D<sub>2</sub> dissociated.

Comparing the RD-SCM displacements for all trajectories (red) to only those that reacted (green), we see very similar curves, both for the x- and y-coordinates. Due to the low reaction probability at curve onset, the data set for the reacted trajectories show a decent amount of noise. This is significantly decreased when looking at the displacement distribution of the reacted slabs near saturation value, although there is still a variation in the results for very low displacements. There also appears to be a slight preference towards a positive displacement even at these higher incidence energies. It is unclear yet why this occurs, although it could be related to the method of generating displacements.

Similar noise is found with the EAM-SCM results for the reacted trajectories at low incidence energy. This, however, disappears when moving towards high energy, or when also including the trajectories that did not react. Furthermore, no clear preference can be found towards a positive or negative displacement, as would be expected for in-plane displacements.

Comparing the two methods to each other, we do see a very clear difference. While both approaches appear to result in a normal distribution of displacements, they have a very different width. The EAM-SCM displacements, obtained from EAM surface slab simulations, showing much broader peaks.

Next, we discuss the most interesting of the three Cartesian directions, the z-coordinate. Displacements towards (+z), or away from (-z), the incoming reactant molecules have in previous works been shown to affect dissociation probabilities[40–43]. For example, Bonfanti *et al.*[40] used a simple 7D model to quantum dynamically show increased reaction probabilities when surface layer atoms are moved away from the incoming H<sub>2</sub> molecule.

In Figures 3.5(a) and 3.5(b), we compare the EAM-SCM and RD-SCM results at reaction probability curve onset for the first and second surface layer atoms. Again only those trajectories that reacted were included separately. For EAM-SCM, reacted trajectories appear to show a clear preference towards a negative displacement in z, away from the D<sub>2</sub> molecule, as the peak of the atom displacement distribution is slightly shifted towards negative z. This phenomena can be observed both for the first layer (a) as well as the second layer (b) and matches results found with the simple 7D model[40]. Interestingly, the opposite effect is found for the CH<sub>4</sub> on Pt(111), Ir(111) and Ni(111) systems, where surface atom displacement away from the reactant increased the barrier

height[41–43]. Furthermore, limited dynamic puckering of the surface atoms is expected away from the bulk when treating this system dynamically, as systems with a large mass mismatch have been shown to be primarily dominated by the the recoil effect[42, 43].

A similar effect can not be seen with the results for the RD-SCM approach, as both the reacted and total surface atom displacements distributions show a similar width and peak location. This distribution also does not appear to be that of a Gaussian. We attribute this to the way the displacements are generated, as it is only ensured the total displacements in the direction of the displacement, and not for the x-, y- or z-axes individually, follows a Gaussian distribution with the standard deviation calculated with the Debye-Waller factor. Similar distributions to that in the z-direction are thus found when looking along the u- and v-axes for the (111) surface slab. Furthermore, the second layer shows a static shift of negative z. This is also attributed to the RD surface slab generation, as experimental interlayer distances are applied when generating the surface, instead of the bulk lattice constant, as is used for the x- and y-directions.

At much higher incidence energies [(c) and (d)], we no longer see the EAM-SCM preference towards a negative z-displacement. At such a high energy, almost all trajectories will react, making the lowest barrier path much less visible. For the RD-SCM results, we again see this second layer shift due to the experimental interlayer distance.

## 3.4 Conclusion

Using the dissociation of  $D_2$  on Cu(111) as a model system, we investigated the physical relevance of the random displacement approach to SCM surface slab generation[23, 24]. Surface slabs were generated using both this approach and a highly accurate EAM potential, which has been shown to accurately describe copper bulk and surfaces[25]. Furthermore, we used this EAM potential to dynamically treat our surface, allowing us to both test the validity of the sudden approach as well as investigate any effect of energy exchange with the surface, which has long been theorised to be of little importance for this system[24]. Each calculation used the same CRP PES based on the SRP48 functional as had been used in previous studies, with the CM approaches all applying the effective 3-body potential as published by Spiering *et al.*[24].

We found good agreement between the dissociation curves of the RD-SCM and the EAM-SCM approaches, as well as with the EAM-DCM approach. Agreement was especially good for reaction curve onset, which has been shown to be the most accurate for experimental results, while the saturation value

was found to be lower for the two methods based on the EAM surface slabs. All three methods resulted in increased broadening of the dissociation S-curve compared to the BOSS approach, which is generally attributed to surface temperature effects.

Similar agreement was found for rovibrational (in)elastic scattering curves, where only the BOSS model significantly deviated from the results found with the different CM approaches. The good agreement between EAM-SCM and EAM-DCM indicated limited to no effect of energy exchange on the reaction and, more importantly, the (in)elastic scattering probabilities. Nevertheless, we did find a drain of 15% of the translational energy of the scattered molecules for almost the entire incidence energy range, which we have not found to be reported in other studies.

A further evaluation of the dissociation curves was performed by simulating a time-of-flight spectrum for each curve, through fitting to the LGS functional form and relying on detailed balance. Such a simulated spectrum is especially sensitive to reaction curve onset, as had been seen in an earlier study[16]. Again we found great agreement between the different CM approaches, as well as improved agreement with experiment[16] compared to the BOSS method.

To directly compare the surface slabs generated for the RD-SCM and EAM-SCM approaches, we mapped the displacements for each individual surface atom from its ideal lattice position, both for all trajectories and only for those trajectories that reacted. As expected, no preference was found for either method when considering the x- and y- coordinate, although the EAM generated slabs did show a much broader distribution of displacements. For the z-coordinate, however, we found a clear preference for reaction when the surface atoms are displaced away from the incoming  $D_2$ , but only for the EAM-SCM approach. Surface slabs generated using the RD-SCM did not even show Gaussian distributions in their displacement, as the displacement method only ensured a normal distribution in the total displacement of the atom.

In general we found good agreement between the reaction probabilities and rovibrational (in)elastic scattering probabilities obtained using the EAM-SCM and RD-SCM approaches, although the RD-SCM approach to surface generation showed much narrower atom displacement distributions. Furthermore, the good agreement with the non-static surface approach of EAM-DCM indicated both the very limited effect of energy exchange on the dissociation and (in)elastic scattering probabilities, despite having observed some energy drain into the surface.

With the success of the SCM sudden approach, combined with physically relevant surfaces generated with an EAM potential, we have opened a pathway towards quantum dynamically treating the motion of  $D_2$  on a non-ideal Cu(111)

---

surface. Accurate quantum dynamically treatment of such systems would be a major step forward in describing the rovibrational (in)elastic scattering as well as the low incidence energy regime, which are dominated by quantum effects ill-described by QCT dynamics.

## References

- (1) Luntz, A. C. In *Chemical Bonding at Surfaces and Interfaces*, Nilsson, A., Pettersson, L. G. M., Nørskov, J. K., Eds.; Elsevier: Amsterdam, 2008, pp 143–254, DOI: [10.1016/B978-044452837-7.50004-6](https://doi.org/10.1016/B978-044452837-7.50004-6).
- (2) Kroes, G.-J.; Somers, M. F. Six-dimensional dynamics of dissociative chemisorption of H<sub>2</sub> on metal surfaces. *Journal of Theoretical and Computational Chemistry* **2005**, *04*, 493–581, DOI: [10.1142/S0219633605001647](https://doi.org/10.1142/S0219633605001647).
- (3) Kroes, G.-J.; Díaz, C. Quantum and classical dynamics of reactive scattering of H<sub>2</sub> from metal surfaces. *Chemical Society Reviews* **2016**, *45*, 3658–3700, DOI: [10.1039/c5cs00336a](https://doi.org/10.1039/c5cs00336a).
- (4) Smith, C.; Hill, A. K.; Torrente-Murciano, L. Current and future role of Haber–Bosch ammonia in a carbon-free energy landscape. *Energy & Environmental Science* **2020**, *13*, 331–344, DOI: [10.1039/C9EE02873K](https://doi.org/10.1039/C9EE02873K).
- (5) Zambelli, T.; Barth, J. V.; Wintterlin, J.; Ertl, G. Complex pathways in dissociative adsorption of oxygen on platinum. *Nature* **1997**, *390*, 495–497, DOI: [10.1038/37329](https://doi.org/10.1038/37329).
- (6) Anger, G.; Winkler, A.; Rendulic, K. D. Adsorption and desorption kinetics in the systems H<sub>2</sub>/Cu(111), H<sub>2</sub>/Cu(110) and H<sub>2</sub>/Cu(100). *Surface Science* **1989**, *220*, 1–17, DOI: [10.1016/0039-6028\(89\)90459-7](https://doi.org/10.1016/0039-6028(89)90459-7).
- (7) Hou, H.; Guldin, S. J.; Rettner, C. T.; Wodtke, A. M.; Auerbach, D. J. The Stereodynamics of a Gas-Surface Reaction. *Science* **1997**, *277*, 80–82, DOI: [10.1126/science.277.5322.80](https://doi.org/10.1126/science.277.5322.80).
- (8) Michelsen, H. A.; Rettner, C. T.; Auerbach, D. J.; Zare, R. N. Effect of rotation on the translational and vibrational energy dependence of the dissociative adsorption of D<sub>2</sub> on Cu(111). *The Journal of Chemical Physics* **1993**, *98*, 8294–8307, DOI: [10.1063/1.464535](https://doi.org/10.1063/1.464535).
- (9) Rettner, C. T.; Michelsen, H. A.; Auerbach, D. J. Quantum-state-specific dynamics of the dissociative adsorption and associative desorption of H<sub>2</sub> at a Cu(111) surface. *The Journal of Chemical Physics* **1995**, *102*, 4625–4641, DOI: [10.1063/1.469511](https://doi.org/10.1063/1.469511).
- (10) Hodgson, A.; Samson, P.; Wight, A.; Cottrell, C. Rotational Excitation and Vibrational Relaxation of H<sub>2</sub> Scattered from Cu(111). *Physical Review Letters* **1997**, *78*, 963–966, DOI: [10.1103/PhysRevLett.78.963](https://doi.org/10.1103/PhysRevLett.78.963).

- (11) Michelsen, H. A.; Auerbach, D. J. A critical examination of data on the dissociative adsorption and associative desorption of hydrogen at copper surfaces. *The Journal of Chemical Physics* **1991**, *94*, 7502–7520, DOI: [10.1063/1.460182](https://doi.org/10.1063/1.460182).
- (12) Cao, K.; Füchsel, G.; Kleyn, A. W.; Juurlink, L. B. F. Hydrogen adsorption and desorption from Cu(111) and Cu(211). *Physical Chemistry Chemical Physics* **2018**, *20*, 22477–22488, DOI: [10.1039/C8CP03386B](https://doi.org/10.1039/C8CP03386B).
- (13) Kaufmann, S.; Shuai, Q.; Auerbach, D. J.; Schwarzer, D.; Wodtke, A. M. Associative desorption of hydrogen isotopologues from copper surfaces: Characterization of two reaction mechanisms. *The Journal of Chemical Physics* **2018**, *148*, 194703, DOI: [10.1063/1.5025666](https://doi.org/10.1063/1.5025666).
- (14) Díaz, C.; Pijper, E.; Olsen, R. A.; Busnengo, H. F.; Auerbach, D. J.; Kroes, G. J. Chemically accurate simulation of a prototypical surface reaction: H<sub>2</sub> dissociation on Cu(111). *Science (New York, N.Y.)* **2009**, *326*, 832–834, DOI: [10.1126/science.1178722](https://doi.org/10.1126/science.1178722).
- (15) Mondal, A.; Wijzenbroek, M.; Bonfanti, M.; Díaz, C.; Kroes, G.-J. Thermal Lattice Expansion Effect on Reactive Scattering of H<sub>2</sub> from Cu(111) at T<sub>s</sub> = 925 K. *The Journal of Physical Chemistry A* **2013**, *117*, 8770–8781, DOI: [10.1021/jp4042183](https://doi.org/10.1021/jp4042183).
- (16) Nattino, F.; Genova, A.; Guijt, M.; Muzas, A. S.; Díaz, C.; Auerbach, D. J.; Kroes, G.-J. Dissociation and recombination of D<sub>2</sub> on Cu(111): ab initio molecular dynamics calculations and improved analysis of desorption experiments. *The Journal of Chemical Physics* **2014**, *141*, 124705, DOI: [10.1063/1.4896058](https://doi.org/10.1063/1.4896058).
- (17) Nattino, F.; Díaz, C.; Jackson, B.; Kroes, G.-J. Effect of Surface Motion on the Rotational Quadrupole Alignment Parameter of D<sub>2</sub> Reacting on Cu(111). *Physical Review Letters* **2012**, *108*, 236104, DOI: [10.1103/PhysRevLett.108.236104](https://doi.org/10.1103/PhysRevLett.108.236104).
- (18) Smeets, E. W. F.; Voss, J.; Kroes, G.-J. Specific Reaction Parameter Density Functional Based on the Meta-Generalized Gradient Approximation: Application to H<sub>2</sub> + Cu(111) and H<sub>2</sub> + Ag(111). *The Journal of Physical Chemistry A* **2019**, *123*, 5395–5406, DOI: [10.1021/acs.jpca.9b02914](https://doi.org/10.1021/acs.jpca.9b02914).
- (19) Wijzenbroek, M.; Klein, D. M.; Smits, B.; Somers, M. F.; Kroes, G.-J. Performance of a Non-Local van der Waals Density Functional on the Dissociation of H<sub>2</sub> on Metal Surfaces. *The Journal of Physical Chemistry A* **2015**, *119*, 12146–12158, DOI: [10.1021/acs.jpca.5b06008](https://doi.org/10.1021/acs.jpca.5b06008).

- 3
- (20) Busnengo, H. F.; Salin, A.; Dong, W. Representation of the 6D potential energy surface for a diatomic molecule near a solid surface. *The Journal of Chemical Physics* **2000**, *112*, 7641–7651, DOI: [10.1063/1.481377](https://doi.org/10.1063/1.481377).
  - (21) Díaz, C.; Olsen, R. A.; Auerbach, D. J.; Kroes, G. J. Six-dimensional dynamics study of reactive and non reactive scattering of H<sub>2</sub> from Cu(111) using a chemically accurate potential energy surface. *Physical Chemistry Chemical Physics* **2010**, *12*, 6499–6519, DOI: [10.1039/C001956A](https://doi.org/10.1039/C001956A).
  - (22) Kroes, G.-J.; Díaz, C.; Pijper, E.; Olsen, R. A.; Auerbach, D. J. Apparent failure of the Born–Oppenheimer static surface model for vibrational excitation of molecular hydrogen on copper. *Proceedings of the National Academy of Sciences* **2010**, *107*, 20881–20886, DOI: [10.1073/pnas.1001098107](https://doi.org/10.1073/pnas.1001098107).
  - (23) Wijzenbroek, M.; Somers, M. F. Static surface temperature effects on the dissociation of H<sub>2</sub> and D<sub>2</sub> on Cu(111). *The Journal of Chemical Physics* **2012**, *137*, 054703, DOI: [10.1063/1.4738956](https://doi.org/10.1063/1.4738956).
  - (24) Spiering, P.; Wijzenbroek, M.; Somers, M. F. An improved static corrugation model. *The Journal of Chemical Physics* **2018**, *149*, 234702, DOI: [10.1063/1.5058271](https://doi.org/10.1063/1.5058271).
  - (25) Sheng, H. W.; Kramer, M. J.; Cadien, A.; Fujita, T.; Chen, M. W. Highly optimized embedded-atom-method potentials for fourteen fcc metals. *Physical Review B* **2011**, *83*, 134118, DOI: [10.1103/PhysRevB.83.134118](https://doi.org/10.1103/PhysRevB.83.134118).
  - (26) Sementa, L.; Wijzenbroek, M.; van Kolck, B. J.; Somers, M. F.; Al-Halabi, A.; Busnengo, H. F.; Olsen, R. A.; Kroes, G. J.; Rutkowski, M.; Thewes, C.; Kleimeier, N. F.; Zacharias, H. Reactive scattering of H<sub>2</sub> from Cu(100): Comparison of dynamics calculations based on the specific reaction parameter approach to density functional theory with experiment. *The Journal of Chemical Physics* **2013**, *138*, 044708, DOI: [10.1063/1.4776224](https://doi.org/10.1063/1.4776224).
  - (27) Füchsel, G.; Cao, K.; Er, S.; Smeets, E. W. F.; Kleyn, A. W.; Juurlink, L. B. F.; Kroes, G.-J. Anomalous Dependence of the Reactivity on the Presence of Steps: Dissociation of D<sub>2</sub> on Cu(211). *The Journal of Physical Chemistry Letters* **2018**, *9*, 170–175.
  - (28) Smeets, E. W. F.; Füchsel, G.; Kroes, G.-J. Quantum Dynamics of Dissociative Chemisorption of H<sub>2</sub> on the Stepped Cu(211) Surface. *The Journal of Physical Chemistry C* **2019**, *123*, 23049–23063, DOI: [10.1021/acs.jpcc.9b06539](https://doi.org/10.1021/acs.jpcc.9b06539).

- (29) Boereboom, J. M.; Wijzenbroek, M.; Somers, M. F.; Kroes, G. J. Towards a specific reaction parameter density functional for reactive scattering of H<sub>2</sub> from Pd(111). *The Journal of Chemical Physics* **2013**, *139*, 244707, DOI: [10.1063/1.4851355](https://doi.org/10.1063/1.4851355).
- (30) Behler, J. First Principles Neural Network Potentials for Reactive Simulations of Large Molecular and Condensed Systems. *Angewandte Chemie International Edition* **2017**, *56*, 12828–12840, DOI: <https://doi.org/10.1002/anie.201703114>.
- (31) Verlet, L. Computer "Experiments" on Classical Fluids. I. Thermodynamical Properties of Lennard-Jones Molecules. *Physical Review* **1967**, *159*, 98–103, DOI: [10.1103/PhysRev.159.98](https://doi.org/10.1103/PhysRev.159.98).
- (32) Berendsen, H. J. C.; Postma, J. P. M.; van Gunsteren, W. F.; Di Nola, A.; Haak, J. R. Molecular dynamics with coupling to an external bath. *The Journal of Chemical Physics* **1984**, *81*, 3684–3690, DOI: [10.1063/1.448118](https://doi.org/10.1063/1.448118).
- (33) Bulirsch, R.; Stoer, J. Numerical treatment of ordinary differential equations by extrapolation methods. *Numerische Mathematik* **1966**, *8*, 1–13, DOI: [10.1007/BF02165234](https://doi.org/10.1007/BF02165234).
- (34) Tsai, D. H. The virial theorem and stress calculation in molecular dynamics. *The Journal of Chemical Physics* **1979**, *70*, 1375–1382, DOI: [10.1063/1.437577](https://doi.org/10.1063/1.437577).
- (35) *Dynamics of Gas-Surface Interactions: Atomic-level Understanding of Scattering Processes at Surfaces*; Muino, R. D., Busnengo, H. F., Eds.; Springer Series in Surface Sciences; Springer-Verlag: Berlin Heidelberg, 2013, DOI: [10.1007/978-3-642-32955-5](https://doi.org/10.1007/978-3-642-32955-5).
- (36) Kroes, G.-J.; Juaristi, J. I.; Alducin, M. Vibrational Excitation of H<sub>2</sub> Scattering from Cu(111): Effects of Surface Temperature and of Allowing Energy Exchange with the Surface. *The Journal of Physical Chemistry C* **2017**, *121*, 13617–13633, DOI: [10.1021/acs.jpcc.7b01096](https://doi.org/10.1021/acs.jpcc.7b01096).
- (37) Dohle, M.; Saalfrank, P. Surface oscillator models for dissociative sticking of molecular hydrogen at non-rigid surfaces. *Surface Science* **1996**, *373*, 14.
- (38) Wang, Z. S.; Darling, G. R.; Holloway, S. The surface temperature dependence of the inelastic scattering and dissociation of hydrogen molecules from metal surfaces. *The Journal of Chemical Physics* **2004**, *120*, 2923–2933, DOI: [10.1063/1.1636724](https://doi.org/10.1063/1.1636724).

- (39) Wijzenbroek, M.; Kroes, G. J. An ab initio molecular dynamics study of D<sub>2</sub> dissociation on CO-precovered Ru(0001). *Physical Chemistry Chemical Physics* **2016**, *18*, 21190–21201, DOI: [10.1039/C6CP00291A](https://doi.org/10.1039/C6CP00291A).
- (40) Bonfanti, M.; Somers, M. F.; Díaz, C.; Busnengo, H. F.; Kroes, G.-J. 7D Quantum Dynamics of H<sub>2</sub> Scattering from Cu(111): The Accuracy of the Phonon Sudden Approximation. *Zeitschrift für Physikalische Chemie* **2013**, 130617035227002, DOI: [10.1524/zpch.2013.0405](https://doi.org/10.1524/zpch.2013.0405).
- (41) Henkelman, G.; Jónsson, H. Theoretical Calculations of Dissociative Adsorption of CH<sub>4</sub> on an Ir(111) Surface. *Physical Review Letters* **2001**, *86*, 664–667, DOI: [10.1103/PhysRevLett.86.664](https://doi.org/10.1103/PhysRevLett.86.664).
- (42) Tiwari, A. K.; Nave, S.; Jackson, B. Methane Dissociation on Ni(111): A New Understanding of the Lattice Effect. *Physical Review Letters* **2009**, *103*, 253201, DOI: [10.1103/PhysRevLett.103.253201](https://doi.org/10.1103/PhysRevLett.103.253201).
- (43) Nave, S.; Jackson, B. Methane dissociation on Ni(111) and Pt(111): Energetic and dynamical studies. *The Journal of Chemical Physics* **2009**, *130*, 054701, DOI: [10.1063/1.3065800](https://doi.org/10.1063/1.3065800).